

# Decision-theoretic MPC: Motion Planning with Weighted Maneuver Preferences Under Uncertainty

Ömer Şahin Taş, *Member, IEEE*, Philipp Heinrich Brusius, and Christoph Stiller, *Fellow, IEEE*

**Abstract**—Continuous optimization based motion planners require deciding on a maneuver homotopy before optimizing the trajectory. Under uncertainty, maneuver intentions of other participants can be unclear, and the vehicle might not be able to decide on the most suitable maneuver. This work introduces a method that incorporates multiple maneuver preferences in planning. It optimizes the trajectory by considering weighted maneuver preferences together with uncertainties ranging from perception to prediction while ensuring the feasibility of a chance-constrained fallback option. Evaluations in both driving experiments and simulation studies show enhanced interaction capabilities and comfort levels compared to conventional planners, which consider only a single maneuver.

**Index Terms**—Planning under uncertainty, risk sensitive planning, interaction-aware planning, safe motion planning.

## I. INTRODUCTION

**A**UTONOMOUS vehicles navigate under uncertain environment information, originating from noisy sensor data and limited field-of-view to unknown future actions of other traffic participants. Despite these uncertainties, they must adhere to their driving objectives and plan a course of motion that is safe and comfortable. This presents a considerable challenge, as sticking to driving preferences and avoiding overly cautious behavior requires quantifying the current risk and responding to unforeseen developments in the current scene. It is thus imperative to evaluate the uncertain environment information, the available route and driving options of other vehicles, as well as the motion limits of the vehicle in the planning process. While these aspects are recognized within the framework of continuous optimization based receding horizon planning, effectively integrating them into a unified planning scheme remains an ongoing challenge.

This work defines motion planning under uncertainty as a model predictive control (MPC) problem. Unlike conventional continuous optimization based motion planners, our framework does not constrain the planned motion profile to a single maneuver homotopy. Instead, it incorporates the preferences on multiple maneuvers by including their variables in its optimization parameters. The resulting motion profile is shaped by weights reflecting these preferences (see figure 1). Furthermore, unlike existing planning approaches, it computes the uncertainty in its fallback motion plan for the current state uncertainty, and ensures the feasibility of the fallback

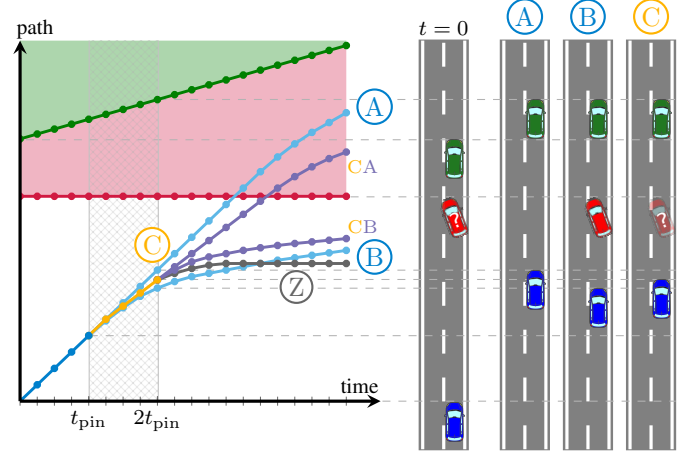


Figure 1: A situation where the existence of the red vehicle is unclear to the blue vehicle. Conventional planners choose a single maneuver homotopy and solve the optimization problem. This results in a motion profile denoted with either maneuver **A** or **B** in the path-time diagram, depicted on the left-hand side. Whenever current information is limited, the vehicle may not have a clear preference on the maneuver homotopy and such a premature decision can result in suboptimal or overly conservative behavior. Decision-theoretic MPC considers preferences and yields profile **C**, which stays within the path range of profiles **A** and **B** in the hatched time interval on the path-time diagram. After  $2t_{pin}$ , it continues with **CA** and **CB**, which will be discarded in the next planning instance. Profile **Z** represents the fallback maneuver guaranteed by profile **C**. The right-hand side depicts profiles **A**, **B** and **C** at  $2t_{pin}$ .

with chance-constraints. This formulation defers maneuver decisions to later times whenever there is no clear preference of a maneuver over the other, facilitating interactive behavior and smooth transitions between distinct maneuver options. We employ gradient-based optimization to solve the resulting nonlinear optimization problem in real-time.

The contributions of this work are as follows:

- Motion planning with continuous optimization that is not constrained to a single maneuver homotopy. The presented formulation inherently blends discrete maneuver decisions with continuous optimization variables, enabling smooth transitions between maneuvers or deferral of the decision under incomplete information.
- Propagation of state uncertainties to the fallback maneuver, and ensuring safety with this fallback maneuver uncertainty in a chance-constrained manner. This complements existing state-dependent collision penalties, enabling proactive yet comfortable navigation under conditions of limited field-of-view and in the presence of rule-violating traffic participants.
- An evaluation of how warm-start solver times and output profiles vary for different vehicle models.

Ömer Şahin Taş and Christoph Stiller are with FZI Research Center for Information Technology and Karlsruhe Institute of Technology (KIT), both 76131 Karlsruhe, Germany. Philipp Heinrich Brusius is with Porsche Motorsport, Dr. Ing. h.c. F. Porsche AG, Ostfildern 73744, Germany. (Corresponding author: Ömer Şahin Taş, e-mail: [tas@fzi.de](mailto:tas@fzi.de)).

- Demonstration of real-time performance through vehicle tests in intersection crossing scenarios. The performance is further validated by simulations leveraging real-world data, and by comparisons with a conventional MPC planner in a distinct scenario.

The remainder of this paper is structured as follows: section II presents related work and identifies open problems within the field of motion planning under uncertainty. Following this, section III introduces our environment model, outlining the assumptions employed therein, which subsequently serve as the foundation for defining safety constraints discussed in section IV. Section V frames motion planning as an optimization problem and outlines the scope of applied constraints. Given the complexity of solving the proposed optimization problem, section VI explores solution approaches. The evaluations of our planning approach are then demonstrated in section VII. The paper concludes with section VIII, highlighting the main contributions of this work and providing directions for future research.

## II. RELATED WORK

Motion planning algorithms should focus on five key objectives: i) arriving at the *destination*, ii) ensuring *comfort*, iii) minimizing *risk*, iv) facilitating *interaction*, and v) conducting *information gathering* [1]. Achieving these objectives require accounting for uncertainties, including i) the uncertainty in *physical state*, which typically covers the uncertainty in position and velocity, ii) the uncertainty in *prediction*, which encompasses the uncertainties in future route choice and intentions, and iii) the uncertainty in *existence*, which reflects the uncertainty of an object to exist, either inside or beyond the field-of-view [2]–[5]. Planning with multiple maneuver options without rendering an overly conservative behavior requires in-depth analysis of existing approaches for safety checks. This is closely related with the approaches for planning motion, as different types of planning algorithms have distinct requirements on the quantification of uncertainties and safety constraints. Therefore, we first inspect existing approaches for performing safety checks and then present planning approaches that maintain safety under uncertainty.

### A. Approaches for Safety Checks Under Uncertainty

Various approaches exist to ensure safety under uncertainty, each with its own set of strengths and limitations. Early work relied on Time-To-X metrics, where “X” represents a selected event such as collision (TTC), the last possible reaction (TTR), or braking (TTB), all measured along the longitudinal dimension [6]–[9]. Later studies aimed to generalize these metrics into Cartesian space [10] and model them as probability distributions [11]–[15]. However, using these metrics for interaction modeling over longer time horizons in urban driving scenarios can rapidly result in complex formulations [16].

In robotics, one common approach to ensure safety is preventing the overlap of an agent’s occupancy with obstacles. While these occupancies can be represented with polygons [17], circles are often preferred because they enable differentiable overlap calculations [18], [19]. However, shapes based

on circles do not inherently correspond to any parametric probability distribution, hence they are primarily used in robust approaches, such as *formal verification*. Variations of these methods, which are employed in autonomous driving, apply set-based over-approximations to all reachable states of traffic participants within a specified environment over a given prediction horizon, and subsequently check for overlaps [20], [21]. A major disadvantage of reachable set-based verification is that over-approximations can quickly grow over time and cause overly conservative behavior.

An alternative approach involves using probability distributions to represent uncertainty. Considering that uncertainties are often modeled as Gaussian distributions, using ellipses for modeling positions becomes a more suitable choice, enabling a direct association with confidence levels [22]. Consequently, this connection allows for closed-form solutions [23], [24] when safety is defined as a chance-constraint [25] with a prescribed risk level. There are alternative ways to constrain the risk, such as Value-at-Risk (VaR) or conditional-VaR [26]. Although these constraints limit the likelihood of an outcome, they do not eliminate its occurrence.

Interaction capabilities between traffic participants are often overlooked while evaluating safety. *Responsibility-Sensitive-Safety* (RSS) addresses this gap and formalizes traffic rules through mathematical models. It ensures safety as long as the vehicles’ motion stays within a set range of parameterized limits [27]. While recent work has extended these models to account for uncertainties and to constrain the associated risk [28], RSS still has a significant drawback. Its reliance on 40 parameters complicates its generalizability [29].

### B. Planners That Aim to Maintain Safety Under Uncertainty

Under uncertainty, absolute safety cannot be guaranteed. Consequently, existing approaches aim to minimize risk. Early examples of motion planners primarily concentrate on state uncertainties and apply probability constraints. They employ either sample-based search methodologies, such as variants of the rapidly-exploring random trees (RRT) [30], [31], or lattice-based search algorithms [32]. A different line of research uses numerical optimization to solve the planning problem and ensures safety via stochastic control techniques [33]–[38]. These methods handle uncertainties in prediction in the same way as they handle state uncertainties. To remain viable for real-time applications, these methods approximate uncertainties with parametric probability distributions.

Several works use reachability analysis to navigate safely under occlusions [39]–[41]. An alternative approach is to leverage formal verification for verifying the presence of a collision-free fallback maneuver until the next planning instance [42]. If the next planning instance cannot ensure safety, the system executes the previously planned fallback maneuver. This strategy is often referred to as *fail-safe* motion planning [43]. A more appropriate approach is to couple the verification of a feasible fallback plan with optimal motion planning. One way to cope with such scenario uncertainties is to integrate the fallback maneuver as a constraint in the numerical optimization problem [44]. The work covers driving

scenarios with uncertain position and speed measurements, and impaired field-of-view. The feasibility of an emergency braking maneuver is ensured amidst these uncertainties by using chance-constraints. Another work takes a similar approach, but instead of addressing uncertainties, it decouples longitudinal and lateral planning to use lateral swerve maneuvers as a fallback [45]. A subsequent work extends this method by considering measurement uncertainties and ensuring safety through chance-constraints [46]. Yet another work focuses on slippery roads and planned fallback maneuvers using a cost function different from the one used for defining optimal motion. This allows the researchers to address uncertainties in road surface friction efficiently [47]. A different work concentrates on performing the decision branching at arbitrary times in the planning horizon [48].

A limited number of works aim to reduce the current uncertainty about the environment, thereby maximizing information content. Some works join disconnected visible areas and rationalize potential traffic participants [49], [50]. Others define the maximization of visible field as an additional driving objective and perform lateral offsetting to increase it [51]. A promising approach is the execution of dedicated actions to actively maximize the vehicle's information of other vehicles' internal states, such as driving intentions [52].

Motion planning under uncertainty can be framed as a partially observable Markov decision process (POMDP). The POMDP framework allows for a seamless integration of state, prediction [53]–[55], and existence uncertainties [56]–[58]. Works using this approach approximate the solution with sampling, which allows them to work with distributions of arbitrary forms and generalizes well to new scenes. However, the complexity of these models increases exponentially with the planning horizon. Therefore, they decide among a limited number of available actions to remain real-time capable. A recent work has analyzed the continuity of the reward in motion planning and leveraged this continuity to speed up planning [59]. Despite this improvement, they are outperformed by planning approaches employing gradient-based optimization in terms of runtime efficiency.

Lastly, there is a growing body of work using deep neural networks to learn the structure of the problem. The approaches that offer safety guarantees are built on the components of existing planning works: they either select a motion plan from a set of safe plans [60], [61] or employ the aforementioned safety check methods to maintain safety under uncertainty [62].

### III. ENVIRONMENT MODEL

An autonomous vehicle operates within a subset of the *world*  $\mathcal{W} \subseteq \mathcal{W}_{\forall}$  that contains a set of objects  $\mathcal{O} = \{\mathbf{o}_0, \dots, \mathbf{o}_{k_{\mathcal{W}}}\}$ , where  $k_{\mathcal{W}} \in \mathbb{N}_0$ . An object  $\mathbf{o}_i$  can belong to a variety of classes, such as cars, pedestrians, cyclists, or even traffic lights. The *state*  $\mathbf{x}_i^{(t)}$  of an object  $i$  stores the relevant parameters necessary to describe the system at time  $t \in \mathbb{N}$ . Sensors of an object  $i$  can perceive only a limited portion of the world  $\mathcal{W}$ , which we refer to as the *environment*  $\mathcal{E}$ . The environment contains a subset of the objects in its

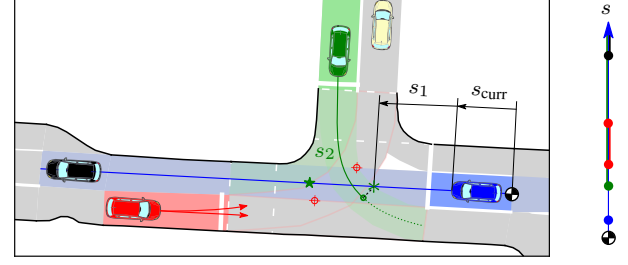


Figure 2: An intersection crossing scene, with the ego vehicle depicted in blue. The longitudinal positions of other vehicles, relative to the ego vehicle's Frenet frame, are marked on a vertical axis to the right of the figure. Considering the red vehicle's two potential routes, the point on the route that is nearest to the ego vehicle's path is considered the start of the overlap. Although the overlap interval for the red vehicle is limited, the overlap with the green vehicle could potentially continue indefinitely, as it could continue driving along the ego vehicle's route.

surroundings  $\mathcal{O}_{\mathcal{E}} = \{\mathbf{o}_i\}_{i=1}^{k_{\mathcal{E}}}$ , where  $k_{\mathcal{E}} \leq k_{\mathcal{W}}$ ,  $k_{\mathcal{E}} \in \mathbb{N}$ , and  $i = 0$  is reserved for the ego vehicle. The environment may include objects that were not detected previously.

Sensor data is typically imperfect, and therefore, state measurements  $\hat{\mathbf{x}}$  carry a degree of uncertainty. These measurements are often modeled with additive noise such that  $\hat{\mathbf{x}} = \mathbf{x} + \zeta_{\mathbf{x}}$ , where  $\zeta_{\mathbf{x}}$  follows a Gaussian distribution with a zero-mean vector and a positive definite covariance matrix, i.e.,  $\zeta_{\mathbf{x}} \sim \mathcal{N}(\mathbf{0}, \Sigma_{\mathbf{x}})$ .

Driving is governed by traffic rules whose applicability typically varies longitudinally along a route. Maps encapsulate critical information about these rules and lane topology. Sections of lanes, where both traffic rules and topology remain consistent, are termed as *lanelets* [63]. Graphs provide a framework for analyzing the relationships between individual lanelets and traffic rules, facilitating the identification of potential conflict areas [64], as depicted in figure 2. Given that traffic rules and interactions primarily depend on longitudinal positions, converting Cartesian coordinates to arc length coordinates along lanelet centerlines, in the *Frenet-Serret frame*, simplifies the analysis of routes and driving intentions of other vehicles. We denote the transformation from Cartesian coordinates to Frenet-coordinates as

$$(s, d) = \mathcal{F}_{\mathcal{C}} M(x, y), \quad (1)$$

and back

$$(x, y) = \mathcal{F}_{\mathcal{F}} M(s, d). \quad (2)$$

It is important to note that this transformation is not always bijective [65].

Analyzing the longitudinal positions using a map facilitates the refinement of the environment with agents that influence decision-making. These objects are referred to as scene objects and denoted by  $\mathcal{O}_{\mathcal{S}}$ , where  $\mathcal{O}_{\mathcal{S}} \subseteq \mathcal{O}_{\mathcal{E}}$ . For instance, in figure 2, the red, green, and black vehicles are considered scene objects, whereas the beige vehicle is not.

Planning requires forecasting the future motion of  $\mathcal{O}_{\mathcal{S}}$  over a specified planning time horizon. This involves two interconnected classification challenges: route prediction and maneuver intention prediction [66], [67]. Distinct maneuver alternatives, or homotopies, are formed by the combinations of these predictions [68]–[70]. Therefore, the number of such

homotopies increases exponentially with the count of participants and the availability of route options [65], [71]. Some works use mixed integer quadratic programming to find the optimal homotopy efficiently [69], [72], [73]. A crucial point to emphasize is that the uncertainty introduced by different homotopies presents a greater challenge for safe planning than the uncertainties within a specific homotopy, due to the greater variability in the state space between homotopies compared with the variability of a single homotopy.

#### IV. MAINTAINING SAFETY UNDER UNCERTAINTY

Given the inherent uncertainty in state measurements, we first address state uncertainty, and then extend the derived formulations to handle both existence and prediction uncertainties.

##### A. State Uncertainty

It is essential to address state uncertainty without rendering an excessively defensive behavior. Related work highlighted using feasible fallback plans as a means of safety in case of a worst-case evolution of the environment. Given uncertain state information, we compute the uncertainty in the fallback plan and leverage chance-constraints to minimize the collision risk under the worst-case event.

The fallback maneuver should be both simple to compute and consistently reduce collision risk when executed. As traffic rules and maneuver intentions are effectively analyzed by road centers, we aim to link fallback plans with longitudinal distances. Therefore, we choose full braking as the fallback plan, taking into account potentially impaired perception and the goal of risk reduction. We limit the distribution of the stop position along the centerline by using chance-constraints. We refer to this full braking maneuver as the *Z-plan*, signifying the vehicle's last available option – ceasing movement. This approach of dealing with uncertainties in the feasibility calculation of the full braking maneuver can promote proactive behavior without compromising safety.

Using full braking as fallback has computational advantages when uncertainties are modeled with Gaussian distributions. A linear transformation of a Gaussian distributed variable  $\mathbf{x} \sim \mathcal{N}(\boldsymbol{\mu}, \boldsymbol{\Sigma})$  results in  $\mathbf{x}_T \sim \mathcal{N}(\mathbf{R}\boldsymbol{\mu} + \mathbf{t}, \mathbf{R}\boldsymbol{\Sigma}\mathbf{R}^\top)$ , where  $\mathbf{R}$  is the rotation matrix and  $\mathbf{t}$  is the translation vector. Since the uncertainties in position and velocity measurements are modeled as an additive zero-mean bivariate Gaussian distribution, projecting them onto a segment of centerline via a unit length vector  $\mathbf{u} \in \mathbb{R}^2$  results in a univariate Gaussian with variance  $\sigma_u^2 = \lambda_u(\boldsymbol{\Sigma}) = \mathbf{u}\boldsymbol{\Sigma}\mathbf{u}^\top$ . This enables the estimation of the current uncertainty in both position and speed along the given centerline, i.e.,  $\hat{s} = s + \zeta_s$  with  $\zeta_s \sim \mathcal{N}(0, \sigma_s^2)$  and  $\hat{v} = v + \zeta_v$  with  $\zeta_v \sim \mathcal{N}(0, \sigma_v^2)$ , respectively. This, in turn, yields braking distance with an additive zero-mean Gaussian noise, if braking distance is linearized using the first-order Taylor expansion

$$F(\mathbf{x}) \approx F(\mathbf{x}^{(0)}) + \nabla F|_{\mathbf{x}^{(0)}}(\mathbf{x} - \mathbf{x}^{(0)}). \quad (3)$$

As  $\mathbf{x}^{(0)} = 0$  for additive Gaussian noise, the variance is obtained as

$$\sigma_F^2 \approx \left(\frac{\partial F}{\partial \mathbf{x}_0}\right)^2 \sigma_{\mathbf{x}_0}^2 + \dots + \left(\frac{\partial F}{\partial \mathbf{x}_{n-1}}\right)^2 \sigma_{\mathbf{x}_{n-1}}^2. \quad (4)$$

For braking distance

$$s_{\text{brake}} = F_{\text{brake}}(v, a^-) = \frac{v^2}{2a^-}, \quad (5)$$

this approximation yields

$$\begin{aligned} \sigma_{\text{brake}}^2 &\approx \left(\frac{\partial F_{\text{brake}}}{\partial v}\right)^2 \sigma_v^2 + \left(\frac{\partial F_{\text{brake}}}{\partial a^-}\right)^2 \sigma_{a^-}^2 \\ &\approx \left(\frac{v}{a^-}\right)^2 \sigma_v^2 + \left(-\frac{v^2}{2(a^-)^2}\right)^2 \sigma_{a^-}^2, \end{aligned} \quad (6)$$

which corresponds to

$$\hat{s}_{\text{brake}} = s_{\text{brake}} + \zeta_{\text{brake}} \quad \text{where } \zeta_{\text{brake}} \sim \mathcal{N}(0, \sigma_{\text{brake}}^2). \quad (7)$$

Because position and braking distance are with an additive white Gaussian noise, stop distance is also with an additive white Gaussian noise

$$\begin{aligned} \hat{s}_{\text{stop}} &= F_{\text{stop}}(s, v, a^-) = \hat{s} + \hat{s}_{\text{brake}} \\ &= s + \zeta_s + s_{\text{brake}} + \zeta_{\text{brake}} \\ &= s_{\text{stop}} + \zeta_{\text{stop}}, \end{aligned} \quad (8)$$

with  $s_{\text{stop}} = s + s_{\text{brake}}$  and  $\zeta_{\text{stop}} \sim \mathcal{N}(0, \sigma_{\text{stop}}^2)$ .

For a vector of random variables  $\mathbf{x}$ , we can constrain the probability that the absolute deviation of a function  $F$  from its expected value does not exceed a certain threshold vector  $\mathbf{t}$

$$\mathbb{P}\left(|F(\mathbf{x} + \boldsymbol{\zeta}_{\mathbf{x}}) - \mathbb{E}(F(\mathbf{x} + \boldsymbol{\zeta}_{\mathbf{x}}))| \leq \mathbf{t}\right) \geq 1 - \alpha, \quad (9)$$

where  $\alpha$  represents a predefined numerical value, often referred to as *risk*. For zero-mean Gaussian noise, this can be expressed as

$$\mathbb{P}(\mathbf{u}_i \hat{\mathbf{x}}_i - \mathbf{t}_i \leq 0) \geq 1 - \alpha, \quad (10)$$

or alternatively as

$$\mathbf{u}_i \mathbf{x}_i + \sqrt{\mathbf{u}_i \boldsymbol{\Sigma}_i \mathbf{u}_i^\top} \cdot \phi^{-1}(1 - \alpha) \leq \mathbf{t}_i, \quad (11)$$

where

$$\phi^{-1}(\gamma) = \sqrt{2} \text{erf}^{-1}(2\gamma - 1).$$

Computationally efficient approximations of the quantile function  $\phi^{-1}$  enable the use of this constraint in real-time applications.

The vehicle  $\vartheta_k$  that is closest to the ego vehicle  $\vartheta_0$  on the current route can be designated as the leader vehicle. We define the worst-case scenario to be when  $\vartheta_k$  initiates full braking immediately after  $\vartheta_0$  processes the environment information. In this worst-case scenario, safety is maintained by ensuring that the difference in the stop positions  $\Delta s_{\text{stop}}$  of both vehicles is less than the standstill distance  $s_{\text{min}}$ . The difference in stop positions can be approximated as

$$\begin{aligned} \Delta s_{\text{stop}} &= F_{\text{stop},0}(s_0, v_0, a^-) - F_{\text{stop},k}(s_k, v_k, a^-) \\ &\approx \hat{s}_{\Delta \text{stop}} = s_{\Delta \text{stop}} + \zeta_{\Delta \text{stop}}, \end{aligned} \quad (12)$$



where  $s_{\Delta\text{stop}} = s_{\text{stop},0} - s_{\text{stop},k}$  and  $\zeta_{\Delta\text{stop}} \sim \mathcal{N}(0, \sigma_{\Delta\text{stop}}^2)$ , such that  $\sigma_{\Delta\text{stop}}^2 = \sigma_{\text{stop},0}^2 + \sigma_{\text{stop},k}^2$ . This implies a chance-constraint of the form

$$\mathbb{P}(\mathbb{1}_{\text{stop}} (\hat{s}_{\Delta\text{stop}} + s_{\text{min}}) \leq 0) \geq 1 - \alpha, \quad (13)$$

where  $\mathbb{1}_{\text{stop}}$  is an indicator function that determines whether the constraint should be activated or not. If  $\mathbb{1}_{\text{stop}}$  equals 1, the constraint is active; otherwise, it is inactive.

### B. Existence Uncertainty

We identify three scenarios as the baseline for safety analysis in the context of existence uncertainty.

1) *Limited visibility*: When no agent is within the visible field-of-view along the driving corridor (see figure 3), the planner must ensure it can stop before reaching the visible free distance  $s_{\text{vis}}$ , while maintaining a safety margin  $s_{\text{min}}$

$$\mathbb{P}(\mathbb{1}_{\text{vis}} (\hat{s}_{\text{stop}} - s_{\text{vis}} + s_{\text{min}}) \leq 0) \geq 1 - \alpha. \quad (14)$$

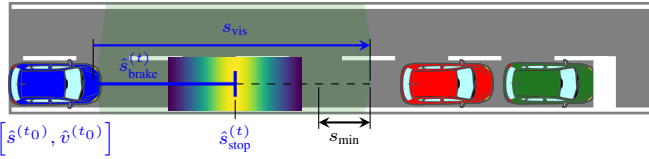


Figure 3: A driving scenario illustrating a limited field-of-view. The braking distance uncertainty of the blue vehicle is represented using a Gaussian distribution.

2) *Limited Visibility at Yield-Intersections*: When the vehicle approaches an intersection where it must yield, and the visible field-of-view is obstructed by buildings or obstacles (see figure 4), the planner must verify whether its visible distance along the intersecting route  $s_{\text{vis}}$  exceeds the required distance  $s_{\text{req}}$  for an oncoming vehicle either to pass or comfortably decelerate to the ego vehicle's speed  $v_0$  while maintaining a time headway  $t_{\text{hw}}$ . The required distance can be computed as

$$s_{\text{req}} = S_{\text{req}}(v_0, v_k, a_{\text{cft}}^-) = v_k t_{\text{dec}} + \frac{1}{2} a_{\text{cft}}^- t_{\text{dec}}^2 + v_0 t_{\text{hw}},$$

by substituting  $t_{\text{dec}} = (v_k - v_0)/|a_{\text{cft}}^-|$  and  $t_{\text{hw}} = 2.0$  s, we get

$$= v_k \left( \frac{v_k - v_0}{|a_{\text{cft}}^-|} \right) + \frac{1}{2} a_{\text{cft}}^- \left( \frac{v_k - v_0}{|a_{\text{cft}}^-|} \right)^2 + 2v_0. \quad (15)$$

If  $s_{\text{vis}} < S_{\text{req}}(v_0, v^+, a_{\text{cft}}^-)$ , the following constraint must hold

$$\mathbb{P}(\mathbb{1}_{\text{yield}} (\hat{s}_{\text{stop}} - s_{\text{MP}} + s_{\text{min}}) \leq 0) \geq 1 - \alpha, \quad (16)$$

which may cause the vehicle to slow down. Otherwise, if  $s_{\text{vis}} \geq S_{\text{req}}(v_0, v^+, a_{\text{cft}}^-)$ , the vehicle can proceed through the intersection – or perform a full stop, if a stop sign is present.

3) *Ambiguous Phantom Detections*: When the existence of a potential phantom object remains unresolved (see figure 1), the constraint defined in equation (13) for state uncertainty must hold.

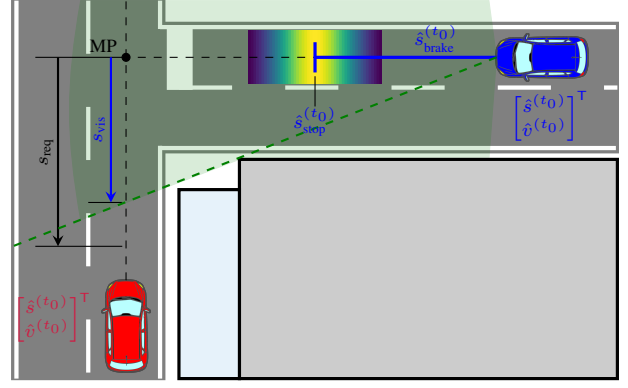


Figure 4: An intersection scenario illustrating a limited field-of-view. The merge point (MP), representing where the routes intersect, is centrally positioned in both corridors for illustrative purposes.

### C. Prediction Uncertainty

In intersection scenarios, the intentions of oncoming vehicles may remain unclear, despite taking into account the applicable traffic rules. Even when the ego vehicle has the right-of-way, thus bearing no responsibility in a potential accident, it should still take into account the possibility of the oncoming vehicle violating traffic rules, if the latter's intentions are not transparent. In such cases, the ego vehicle should satisfy the constraint in equation (14). Moreover, equation (15) can be employed to infer whether the oncoming vehicle intends to yield or not.

## V. DECISION-THEORETIC MODEL PREDICTIVE CONTROL

Our proposed method involves finding an optimal action sequence that minimizes an objective function under safety constraints in a receding horizon. We present these individual aspects before introducing our planner.

### A. Safety in Receding Horizon Planning

A planning horizon of length  $t_h$  using a sampling interval of  $t_s$  can be approximated by  $n$  collocation points, also referred to as *trajectory support points*. These points are denoted by  $\mathbf{p}_i = [\mathbf{x}_i, \mathbf{a}_i]$  with  $0 \leq i \leq n$ , where  $\mathbf{x}$  and  $\mathbf{a}$  represent states and actions, respectively. The number of points that can be freely adjusted during optimization is not equal to  $n$ , as during computation  $t_c$ , a number of control inputs,  $k = \lceil t_{\text{pin}}/t_s \rceil$  with  $t_c \leq t_{\text{pin}}$ , must be held fixed for temporal stability.

In the next replanning instance, the first  $k$  parameters from the current instance will be discarded, and the parameters from  $k$  to  $2k$  will be held fixed. The optimization parameter vector can thus be represented as

$$\mathbf{p} = [\underbrace{\mathbf{p}_0}_{\text{pinned}}, \underbrace{\mathbf{p}_{1:k}}_{\text{executed next}}, \underbrace{\mathbf{p}_{k+1:2k}}_{\text{will be recalculated}}, \underbrace{\mathbf{p}_{2k+1:n}}_{\text{will be recalculated}}]. \quad (17)$$

Though  $\mathbf{p}_0$  represents the current measurement, we include it in the parameter vector for the sake of completeness.

Since the actions up to  $2k$  are irreversible, it is crucial for the planner to ensure none of these actions result in an *inevitable collision state* beyond this interval [42], [44]. For this purpose, we apply the stop distance chance-constraints, discussed in

the previous section, within this time interval. Additionally, to avert immediate collisions, we apply circle-to-ellipse hard constraints

$$\bigwedge_{o \in \mathcal{O}_S} \sqrt{\left(\frac{x_o - x}{\sigma_x + \delta}\right)^2 + \left(\frac{y_o - y}{\sigma_y + \delta}\right)^2} > 1, \quad (18)$$

where circles encompass the occupancy of the vehicle, and ellipses represent the uncertainty in the position of objects [22].

### B. Vehicle Models

The trajectory support points must adhere to the non-holonomic motion constraints of the vehicle. There are various vehicle models to capture the nonlinear dynamics of the system  $\dot{\mathbf{x}} = \mathbf{g}_{\text{veh}}(\mathbf{x}, \mathbf{a})$  [74]–[76]. In our evaluation, we benchmark several models, including the point mass, the kinematic bicycle, the linear kinematic bicycle, and the dynamic bicycle model with linear tire model. For the sake of simplicity, we use  $\mathbf{x} = [x, y, \psi, v]$  and  $\mathbf{a} = [\delta, a]$ , regardless of the underlying motion model. We integrate piecewise constant actions with the classic Runge-Kutta method.

### C. Driving Objectives and Cost Function

We define three types of cost term templates for rendering comfortable and safe driving objectives [77]. These include value terms that penalize deviations from a desired value  $x^*$

$$J_{\text{val}}(x) = w_{\text{val}} \|\mathbf{x}^* - x\|^2, \quad (19a)$$

range terms, that penalize values outside of an interval described by a lower bound  $x^-$  and an upper bound  $x^+$

$$J_{\text{ran}}(x) = \begin{cases} w_{\text{ran}} \|x - x^+\|^2 & \text{if } x^+ < x \\ 0 & \text{if } x^- \leq x \leq x^+ \\ w_{\text{ran}} \|x - x^-\|^2 & \text{otherwise,} \end{cases} \quad (19b)$$

and an asymmetric loss around  $x^*$

$$J_{\text{asym}}(x) = \begin{cases} w_{\text{asym}} \|x - x^*\|^2 & \text{if } x \geq x^* \\ w_{\text{asym}} \log(1 + \|x - x^*\|^2) & \text{otherwise,} \end{cases} \quad (19c)$$

where lower values are penalized with a tolerant loss, such as the Cauchy loss [78]. It is important to note that both  $J_{\text{ran}}$  and  $J_{\text{asym}}$  include conditional statements.

We define the total costs for planning as

$$J_{\text{total}}(\mathbf{p}) = J_{\text{drive}}(\mathbf{p}) + J_{\text{comf}}(\mathbf{p}) + J_{\text{coll}}(\mathbf{p}). \quad (20)$$

The first term

$$J_{\text{drive}}(\mathbf{p}) = \sum_{i=0}^n J_{\text{asym}}(v_i) \quad (21)$$

aims to align the speed values  $v$  in the state vector  $\mathbf{x}$  with the desired travel speed  $v_{\text{des}}$ , which is set to 90% of the speed limit. Speeds exceeding the maximum allowed are penalized with quadratic loss, while slower speeds, as common in dense traffic, are penalized with the tolerant loss. The second term

$$J_{\text{comf}}(\mathbf{p}) = J_{\text{val}}(\mathbf{a}_a) + J_{\text{val}}(\mathbf{a}_{\text{lat}}) + J_{\text{val}}(\mathbf{j}) \\ + J_{\text{ran}}(\mathbf{a}_a) + J_{\text{ran}}(\mathbf{a}_{\text{lat}}) + J_{\text{ran}}(\mathbf{j}) \quad (22)$$

ensures comfortable driving. Here,  $\mathbf{a}_a$  represents the longitudinal accelerations,  $\mathbf{a}_{\text{lat}}$  represents the lateral accelerations (calculated using the vehicle model), and  $\mathbf{j}$  represents the jerk values (calculated from  $\mathbf{a}_a$  using finite differences). Lateral acceleration is penalized separately from its longitudinal counterpart to control the vehicle's lateral maneuvering behavior. The optimal values for all these comfort terms are zero. The third term

$$J_{\text{coll}}(\mathbf{p}) = w_{\text{coll}} \sum_{o \in \mathcal{O}_S} \left[ \left( 1 + \text{erf} \left( \frac{(s - s_o)}{\sqrt{2\lambda_{\text{lon}}(\Sigma_o)}} \right) \right) \right. \\ \left. \left( 1 + \text{erf} \left( \frac{(d - d_o)}{\sqrt{2\lambda_{\text{lat}}(\Sigma_o)}} \right) \right) \right] \quad (23)$$

penalizes collision risks with scene objects by projecting their uncertainties onto the reference path.

### D. Model Predictive Contouring Control (MPCC)

Instead of repeatedly calculating the longitudinal position  $s$  for the purpose of analyzing interactions and traffic rules, the MPCC formulation [79], [80] directly integrates it into the state  $\mathbf{x}_{\text{mpcc}} = [\mathbf{x}, s]$ , while incorporating its derivative – the projected speed along the route – into the action variables  $\mathbf{a}_{\text{mpcc}} = [\mathbf{a}, \dot{s}]$ . The formulation first determines the reference Cartesian coordinates and the corresponding yaw angle  $(x^{\text{ref}}(s_i), y^{\text{ref}}(s_i), \psi^{\text{ref}}(s_i))$  for the desired longitudinal positions. Subsequently, as part of the optimization process, it computes the longitudinal and lateral contouring errors

$$e_{\text{lon}} = -(x^{\text{ref}} - x) \sin(\psi^{\text{ref}}) + (y^{\text{ref}} - y) \cos(\psi^{\text{ref}}) \quad (24a)$$

$$e_{\text{lat}} = (x^{\text{ref}} - x) \cos(\psi^{\text{ref}}) + (y^{\text{ref}} - y) \sin(\psi^{\text{ref}}). \quad (24b)$$

These errors are calculated within a coordinate frame that aligns with the tangent vector at the reference coordinates, as illustrated in figure 5. The deviations build up the costs

$$J_{\text{mpcc}}(\mathbf{p}) = J_{\text{val}}(e_{\text{lon}}) + J_{\text{val}}(e_{\text{lat}}) + J_{\text{val}}(\dot{s}). \quad (25)$$

Notably, these cost terms complement the loss term defined in equation (21).

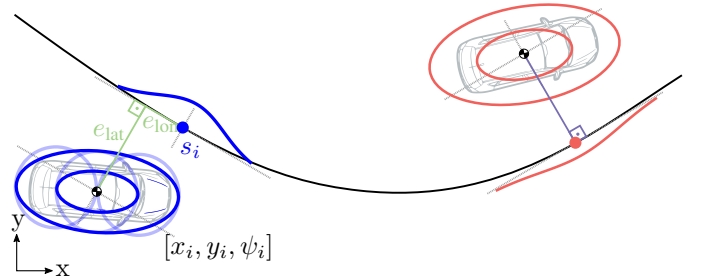


Figure 5: Uncertainty projection in conjunction with the MPCC formulation.

With the MPCC formulation in place, we augment the total cost function outlined in equation (20) as

$$J_{\text{total}}(\mathbf{p}) = J_{\text{drive}}(\mathbf{p}) + J_{\text{comf}}(\mathbf{p}) + J_{\text{coll}}(\mathbf{p}) + J_{\text{mpcc}}(\mathbf{p}). \quad (26)$$

In addition, the formulation imposes further constraints on  $e_{\text{lon}}$  and  $e_{\text{lat}}$ , confining them within an interval defined by upper and lower bounds. It is worth emphasizing that, while

the reference coordinates and tangent vectors in the MPCC formulation serve for error calculation, our approach further leverages them for projecting uncertainties.

### E. Incorporating Maneuver Preferences in MPC Framework

Planning amidst unclear maneuver intentions from others introduces a high level of uncertainty, as previously discussed. Particularly for continuous optimization based planners, the challenge lies in the necessity of committing to a single maneuver, or homotopy, before optimizing motion within it. A practical alternative is to consider all maneuvers simultaneously with their preference scores, or weights, and plan a motion accordingly. This approach enables the planner to optimize a motion profile that is not confined to a single homotopy, but rather, is *homotopy-free* or *maneuver-neutral* [5], [81].

We augment the parameter vector of the planning problem by incorporating state and action parameters that correspond to distinct available maneuvers. In the case of two maneuvers A and B, this modification yields the parameter vector

$$\mathbf{p}^* = [\underbrace{\mathbf{p}_0, \mathbf{p}_{1:k}}_{\text{pinned}}, \underbrace{\mathbf{p}_{k+1:2k}}_{\text{executed next}}, \underbrace{\mathbf{p}_{2k+1:n}}_{\text{will be recalculated}}, \underbrace{\mathbf{p}_{n+1:2n-2k}}_{\text{will be recalculated}}]. \quad (27)$$

The braces C, CA, and CB represent the segments of the maneuver on the path-time diagram shown in figure 1. It should be noted that this planning scheme requires  $(n - 2k)(\dim(\mathbf{x}) + \dim(\mathbf{a}))$  additional parameters for each extra maneuver considered. However, in many situations, the number of alternative maneuver options can be reduced to two.

Despite modifications to the parameter vector, we preserve the original form of both the cost and constraint functions. We, therefore, feed parameters into these functions such that they represent individual maneuvers. Given two distinct maneuver options A and B, the schema for parameter passing is

$$\mathbf{p}_A^* = [\mathbf{p}_{0:k}, \mathbf{p}_{k+1:2k}, \mathbf{p}_{2k+1:n}], \quad (28a)$$

$$\mathbf{p}_B^* = [\mathbf{p}_{0:k}, \mathbf{p}_{k+1:2k}, \mathbf{p}_{n+1:2n-2k}]. \quad (28b)$$

We compute the total cost as a weighted sum

$$J_{\text{total}}^* = w_A J_{\text{total}}(\mathbf{p}_A^*) + w_B J_{\text{total}}(\mathbf{p}_B^*). \quad (29)$$

The maneuver weights  $w_{(\cdot)}$  are assigned by a decision function  $F_{\text{DT}}$  based on the current scene.  $F_{\text{DT}}$  can represent a model-based or a learning-based approach. In this work, we do not delve into the design of the optimal decision function, but use the maneuver probabilities or the existence probabilities of other participants as maneuver weights.

This planning framework does not compromise safety, because if motion profiles A and B obtained by a conventional planner are safe  $\forall i \in \{k + 1, \dots, 2k\}$ , then there is a motion profile C, such that  $\mathbf{s}_{B,i} \leq \mathbf{s}_{C,i} \leq \mathbf{s}_{A,i}$ , that is also safe  $\forall i \in \{k + 1, \dots, 2k\}$ .

It is important to underscore that this formulation enables the planner to postpone decisions, taking advantage of the expectation that more information will be available in the future. Consequently, we term this capability as *passive* information gathering.

### F. Decision-Theoretic MPC

The outlined planning approach with maneuver preferences in the preceding subsection forms the core of *decision-theoretic MPC*. However, relying solely on this core formulation could potentially result in actions that exhibit undesired behavior, unless further constraints are introduced to better guide the optimization. Consequently, we integrate safety constraints for the system and name this formulation as decision-theoretic MPC<sup>1</sup>. In our application, this results in

$$\min_{\mathbf{p}^*} w_A J_{\text{total}}(\mathbf{p}_A^*) + w_B J_{\text{total}}(\mathbf{p}_B^*) \quad (30a)$$

$$\text{s.t. } \mathbf{h}_{\text{dyn}}(\mathbf{p}_A^*) = \mathbf{0}, \quad (30b)$$

$$\mathbf{h}_{\text{dyn}}(\mathbf{p}_B^*) = \mathbf{0}, \quad (30c)$$

$$\mathbf{g}_{\text{acc}}(\mathbf{p}_A^*) \leq \mathbf{0}, \quad (30d)$$

$$\mathbf{g}_{\text{acc}}(\mathbf{p}_B^*) \leq \mathbf{0}, \quad (30e)$$

$$\mathbf{g}_{\text{cnt}}(\mathbf{p}_A^*) \leq \mathbf{0}, \quad (30f)$$

$$\mathbf{g}_{\text{cnt}}(\mathbf{p}_B^*) \leq \mathbf{0}, \quad (30g)$$

$$G_{\text{crc}}(\mathbf{p}_i^*) \leq 0, \quad \forall i \in \{0, \dots, 2k\} \quad (30h)$$

$$G_{\text{chn}}(\mathbf{p}_i^*) \leq 0. \quad \forall i \in \{0, \dots, 2k\} \quad (30i)$$

Here, the objective function directly employs equation (29), which is a weighted sum of the costs in equation (26). The constraint  $\mathbf{h}_{\text{dyn}}$  represents the vehicle motion models referenced in section V-B,  $\mathbf{g}_{\text{acc}}$  denotes longitudinal and lateral acceleration limits,  $\mathbf{g}_{\text{cnt}}$  denotes the longitudinal and lateral contouring error constraints introduced in section V-D,  $G_{\text{crc}}$  denotes the circle-to-ellipse safety constraint defined in equation (18). Lastly,  $G_{\text{chn}}$  represents the chance constraints, composed of

$$G_{\text{chn}}(\mathbf{p}) = G_{\text{stop}}(\mathbf{p}) \wedge G_{\text{vis}}(\mathbf{p}) \wedge G_{\text{yield}}(\mathbf{p}), \quad (31)$$

where its respective components are defined in equations (13), (14) and (16).

It is important to note that this formulation does not enforce any constraints for obstacle avoidance beyond the index  $k$ . This is a sensible approach, given that newly detected objects beyond this index could invalidate the preceding solution used for initialization at the current planning instance, potentially causing the optimization routine to fail.

### VI. SOLVING LOCAL-OPTIMIZATION PROBLEMS

The optimization problem presented is not only complex, but it also must be solved in real-time. For this reason, we use an Interior Point Method (IPM), a type of second-order gradient-based nonlinear optimization algorithm [83]–[85]. IPMs transform inequality constraints into equality constraints by introducing slack variables and define a logarithmic barrier term to satisfy these constraints. As the optimization process progresses, the value of the barrier term is reduced until the Karush-Kuhn-Tucker conditions for an equality-constrained problem are met. This procedure imparts robustness to IPMs, eliminating feasibility requirements on initialization.

We use the IPM solver IPOPT [86], known as the most powerful and robust nonlinear solver available. It is a primal-dual algorithm and features a “filter” line search method, a

<sup>1</sup>We refrain from abbreviating our method as DTMPCC to avoid confusion with dynamic tube MPC [82].

second-order correction method for the step factor selection, and inertia correction capabilities which enable its robust operation. Whenever it cannot find a feasible line search step factor, it enters into restoration mode and minimizes the constraint violation.

The presented optimization problem has many optimization parameters and constraints, thereby making the calculation of gradients and Hessians more challenging. Various methods for computing gradients and Hessians are compared in table I. We choose automatic differentiation for its flexibility and efficiency [87]. Among the automatic differentiation libraries available for the C++ programming language, CppAD [88] and CasADi [89] are the most powerful. They both employ sparse-matrix methods to reduce the storage and computational overhead. The main advantage of CppAD over CasADi lies in its ability to be integrated into templated function definitions, thus blending into existing software without requiring a complete rewrite. We assess the performance of both libraries in our benchmarks.

Derivative Method	Accuracy	Speed	Setup Time	Error Safe
Analytical Deriv.	+++	++	-	-
Numeric Diff.	-	-	+++	+++
Symbolic Diff.	+++	+	+	++
Automatic Diff.	+++	+	++	++
Hybrid Auto. Diff.	+++	+++	++	++

Table I: Comparison of various differentiation methods [90], [91].

From the comparison presented in the table above, it is apparent that hybrid automatic differentiation, e.g., CppADCodeGen [92], shows better performance over standard automatic differentiation. This is because CppAD operates on scalars rather than matrices and does not benefit from advanced compiler optimization techniques. Although this results in a slightly worse performance, the generated code is dependency-free, facilitating its operation on embedded systems and GPUs. Additionally, it allows static memory allocation, enabling hard real-time guarantees [90], [91].

## VII. EVALUATION

We demonstrate the efficacy of our motion planner in both simulation studies and driving experiments. In our evaluations, we set  $t_s = 100$  ms and  $t_h = 6$  s. Additionally, we set the number of pinned control inputs  $k$  to 2, except in the phantom object scenario, where we use a value of 4.

To evaluate safe intersection crossing under impaired perception, we examine a scenario where a vehicle's visible field-of-view is obstructed by surrounding buildings (see figure 6). Initially, the vehicle is unaware of the intersection at which it must yield to vehicles approaching from other directions. We analyze speed profiles for various sensor ranges on a path-speed diagram and define the center of the intersection as the origin of the path axis.

Speed profiles indicate that with longer sensor ranges, the vehicle can detect the intersection sooner, enabling a more comfortable reduction in speed. On the other hand, with shorter sensor ranges, the vehicle identifies the intersecting route closer to the intersection and later in time, resulting in

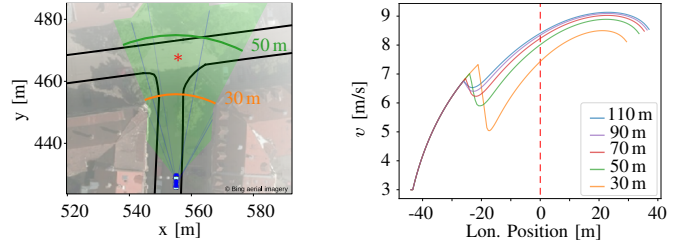


Figure 6: Trajectories at an intersection crossing for various sensor ranges.

a harsher deceleration. Note that all profiles on the diagram are of the same length, as the simulation is run for the same time period. Once the vehicle has enough visible field in the intersection area, all profiles accelerate and reach a peak speed at approximately 20m past the center of the intersection. Afterwards, they decelerate due to the limited field-of-view resulting from the presence of buildings and the curvature of the road. This implies that sensor ranges exceeding 50 m may not always be advantageous in urban driving.

We evaluate the motion of our decision-theoretic MPC in certain challenging scenarios. These include an S-shaped swerve scenario and a 180°-cornering, each with objects divided into two groups (see figure 11 and figure 12 in the appendix). Only one of the groups actually exists in reality, but this is unknown to the planner. Therefore, the vehicle has no preference on the corresponding maneuver options and weights them equally. The resulting motion is optimized for both options in the immediate time horizon, and it maintains a sufficient distance from all obstacles. Having identical motion in the immediate time horizon across different maneuvers is a distinguishing feature of the decision-theoretic MPC.

In some situations, environmental constraints might prevent the execution of swerve maneuvers, leaving braking as the only viable option. Such a situation is illustrated in figure 1, where the vehicle detects a vehicle with a 50 % existence probability, moving at 2.0 m/s, located 15.0 m ahead. We evaluate two variations of this scenario: in the first, the phantom detection is resolved after 0.3 s, while in the second, its existence remains unclear. The comparison between the decision-theoretic MPC and a conventional planner is depicted in figure 7. While the conventional planner calculates the motion by assuming the phantom to be valid, the decision-theoretic planner assesses the likelihood of a phantom presence and assigns  $w_A = 0.5$  and  $w_B = 0.5$  to the braking and driving straight maneuver options, respectively. By ensuring the feasibility of a fallback maneuver, it reacts more comfortably to the phantom without compromising safety. The slight jump in the left subfigure results from the change of the reference contour in the MPCC formulation.

Our decision-theoretic MPC is capable of proactively handling rule-violating behaviors by other vehicles. This ability is showcased through driving experiments performed at a T-intersection, where the autonomous vehicle has the right-of-way, and an oncoming vehicle must yield to it (see figure 8). To introduce variability in the experiment and prove the robustness of our algorithm, the oncoming black vehicle is driven manually. It approaches the intersection at a speed that



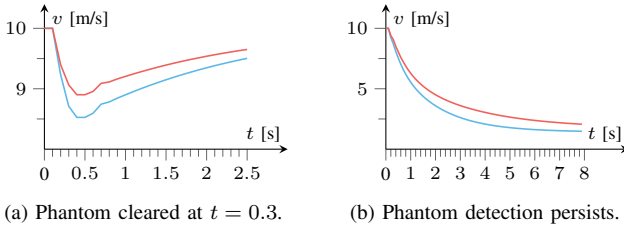


Figure 7: A comparison of executed speed profiles between the decision-theoretic MPC (—) and a conventional MPC (—) in the phantom object detection scenario. While the conventional planner calculates the motion by assuming the phantom to be valid, the decision-theoretic planner assesses the likelihood of a phantom presence.

suggests it will not yield to the autonomous gray vehicle, yet brakes at the very last moment. To isolate the effect of perception artifacts, the black vehicle transmits its position and speed via V2V-communication to the autonomous vehicle CoCar [93].

Figure 8 presents a sequence of frames extracted from a video of a test run. The autonomous vehicle uses the probability of the other vehicle crossing the intersection as the preference weights for its maneuver options. Fallback plans, i.e., the braking trajectories ensuring a full stop before the intersection, are depicted in figure 9. The vehicle, realizing that the black vehicle will not be able to stop comfortably to yield, retains its stop constraint defined in equation (16). The active full stop constraint subtly reduces the vehicle’s speed as it nears the intersection. Once it becomes clear that the oncoming vehicle will yield to the autonomous vehicle, the constraint is released.

The cost function of the decision-theoretic MPC enables interactive behavior and smooth transitions between distinct maneuvers, despite changing predictions and driving goals. We evaluate these characteristics, among its other features, such as planning with a limited field-of-view, in the free and open source simulation environment P3IV [94]. Figure 10 illustrates a planning instance from a roundabout scenario [95]. The vehicle evaluates the probabilities of distinct maneuver options of other vehicles with a particle filter-based prediction module and plans a trajectory accordingly. The figure consists of three subplots: 1) most likely predictions of vehicles in the scene model together with the planned motion on a path-time diagram, 2) vehicle positions and uncertainties at the time of planning, and 3) the profile of the planned motion. These results showcase consistently smooth motion profiles in the immediate time horizon.

One of the major challenges in the development of planning algorithms using numerical optimization lies in problem modeling and initialization. Besides the modeled objective function, the underlying dynamic model can considerably influence the solution. Therefore, we evaluate the runtimes of various vehicle models during replanning for different initializations. Table II presents results using an Intel i7-4710MQ CPU. While it is intuitive that models of greater complexity result in higher runtimes, it is surprising to note that the linear kinematic vehicle model can, under certain conditions, display poor convergence and have significantly higher runtimes. This

occurs when the initialization, and thus the linearization, is distant from the optimum. Given the need to incorporate new environment information during replanning, linearization within receding horizon planning can be a delicate task. We provide a qualitative comparison of the kinematic vehicle model and dynamic vehicle model in figure 13 and figure 14 in the appendix. In addition to comparing vehicle models, we examine the difference in runtimes between classic Runge-Kutta and Euler’s method as integration schemes. Our evaluations reveal that the differences in runtimes were negligible.

Model	S-Shaped (free)		S-Shaped		180°- Corner	
	Avg.	Max	Avg.	Max	Avg.	Max
Point Mass	21.25	23.16	50.78	75.21	57.68	91.86
Kinematic	26.73	39.95	53.38	91.76	56.82	83.66
Linear Kin.	27.08	33.55	67.37	759.09	69.19	183.52
Dynamic	57.91	85.95	115.84	194.49	123.24	184.21

Table II: Comparison of solver times in ms for various vehicle models across different scenarios during replanning. The scenarios are depicted in figure 13 and figure 14 in the appendix.

Nonlinear optimization algorithms use linear solvers to solve linearized subproblems. In our runtime analysis, the linear solvers MUMPS [96], MA27, MA57 [97] performed comparably. Further qualitative runtime evaluations showed that merely 10%–15% of the solution time was spent on calculating derivatives. Despite some works reporting a superior performance of CppAD over CasADi, our experiments did not reveal any significant difference in runtimes.

The computation of the exact Hessian in each iteration carries an additional computational overhead. Quasi-Newton methods approximate the Hessian, thereby reducing computational cost and memory requirements at the cost of some accuracy and convergence speed. Our evaluations demonstrated marginally better runtimes favoring full Newton methods.

In our safety modeling, we employ full braking maneuvers as a fallback strategy. Swerving is an alternative strategy; however, using it for collision avoidance under uncertainty poses two significant problems: Firstly, vehicle models are often linearized for Gaussian error propagation and uncertainty modeling. This could lead to substantial modeling errors when executing maneuvers at the vehicle’s handling limits. Secondly, the area used during swerving might overlap with the occupancy of objects located beyond the visible field.

In motion planning for autonomous driving, certain works use predicted motion profiles of objects to narrow the drivable corridor and address collision avoidance [19]. Although this approach potentially allows for faster solver times, it hinders the motion planner from processing the environment probabilistically, thereby limiting its interaction capabilities. Therefore, we did not adopt this approach in our work.

During our development process, we also analyzed the use of a continuously differentiable distance function [19] to directly calculate longitudinal positions from Cartesian coordinates, as defined in equation (1). While this approach initially seemed promising, especially in problems with conflicting objectives, it occasionally led to poor convergence, resulting in unstable behavior.





Figure 8: Safe intersection crossing in the presence of rule-violating participants. The autonomous vehicle (gray) has the right of way. However, the speed of the oncoming black vehicle suggests it will not yield. The gray vehicle reduces its speed to satisfy the full stop constraint before the intersection. Once it becomes clear that the black vehicle will yield, it accelerates back to its desired driving speed. Frames are incremented every 0.25 s.

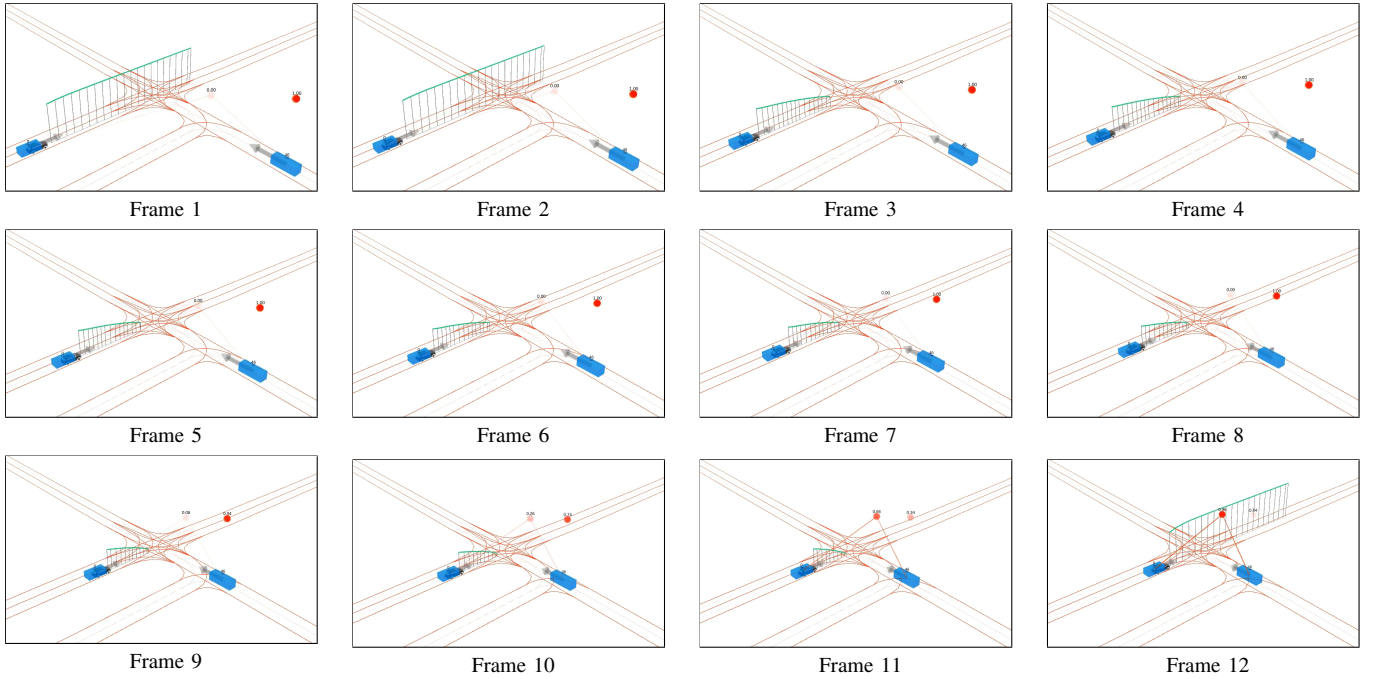


Figure 9: Fallback plans during the intersection crossing scenario in RViz.<sup>2</sup> Frames 3 to 11 illustrate the vehicle's deceleration, ensuring the feasibility of a full stop before reaching the intersection. The probability of the black vehicle crossing is displayed at the top of the red circle. Frames are incremented every 0.25 s, but their numbering is not synchronized with the camera image frames from the previous figure.

<sup>2</sup>Video available online at <https://youtu.be/1OpE5uldJil>

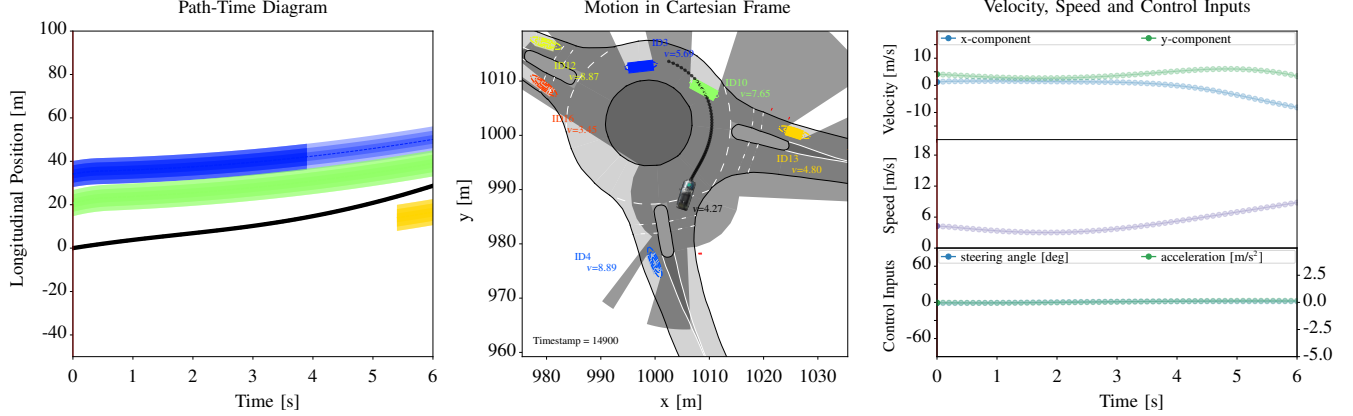


Figure 10: An intersection crossing scenario with multiple vehicles. The ego vehicle is depicted in black, while the vehicles in the environment model  $\mathcal{O}_E$  are shown with their position uncertainty and have a semi-transparent rectangle centered at their mean position. Vehicles in the scene model  $\mathcal{O}_S$  are depicted with opaque rectangles. Despite visibility constraints, uncertainty in perception and prediction, the decision-theoretic MPC plans smooth motion profiles and crosses the roundabout.<sup>3</sup>

Finally, it is crucial to emphasize that the replanning time  $t_c$  directly affects the ability to reach the desired speed in receding horizon planning under safety constraints. Ensuring a feasible fallback plan within  $t_c$  can prevent reaching desired travel speeds, especially when the replanning time is long and the field-of-view is limited.

## VIII. CONCLUSION

Uncertainties due to impaired perception and partial observability often lead to defensive plans. In this work, we developed a planning approach that eliminates the need to determine the best homotopy in advance. Instead, it incorporates homotopy preferences in planning. In this way, it couples decision making with local continuous optimization.

In the context of autonomous driving, our approach can produce homotopy-free or maneuver-neutral motion that serves as an intermediate choice between distinct maneuver alternatives. We have paired this approach with inevitable collision states to develop a proactive, chance-constrained safe motion planning formulation. Consequently, it offsets the limitations of perception and prediction while maintaining interaction-aware driving and safety. Evaluations from both driving experiments and simulations derived from real-world driving scenarios demonstrate that the presented approach proves particularly beneficial whenever the current environment information entails significant levels of uncertainty.

In this work, our focus was primarily on urban driving scenarios, though the formulations presented can be seamlessly extended to highway lane-change situations. While our evaluations centered around traffic participants that are vehicles, the approach remains adaptable to other types, such as cyclists and pedestrians. One limitation of the present work is that we restricted ourselves to only two maneuver alternatives. The extension to more than two maneuvers involves additional steps. Firstly, environment modeling and the identification of non-conflicting maneuvers can become complex. Secondly, as

the computational complexity increases with the number of optimization parameters, maintaining a sufficient planning rate might become challenging. Future work could use a learning-based approach to identify maneuver preferences and compare the resulting planner with end-to-end planning approaches.

## ACKNOWLEDGMENTS

We thank Ole Salscheider for setting up the vehicle-to-vehicle communication and Florian Kuhnt for providing motion predictions for the vehicle experiments. We further thank Mykel J. Kochenderfer for his insightful discussions and comprehensive review on this work.

<sup>3</sup>Video available online at <https://youtu.be/iqZvPMBpUZQ>

## APPENDIX

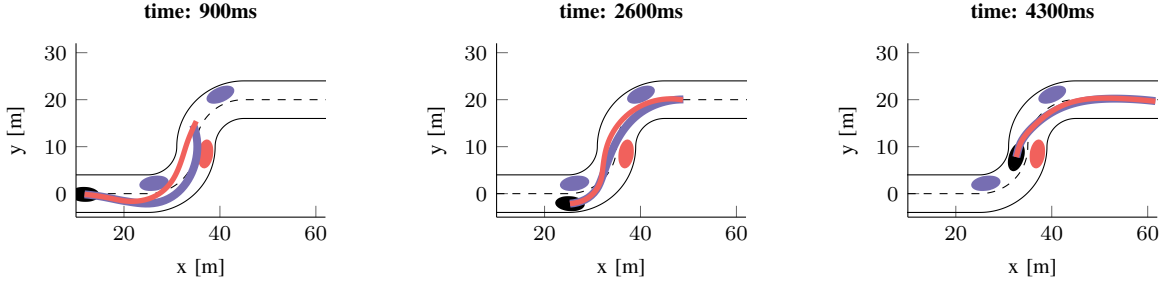


Figure 11: Simulation results in an S-shaped corridor with obstacles of uncertain existence. The obstacles are divided into two groups, but only one group actually exists in reality. The vehicle is unaware of which group is real, and thus, treats the corresponding maneuver options with equal preference. The color of each maneuver option match the color of obstacles considered during planning. To ensure safety and prevent potential collisions, all obstacles are accounted for in the time interval  $[0, t_{2pin}]$ . For this reason, the corresponding trajectories maintain a sufficient distance from the obstacles. Unlike conventional MPCs, the first few meters of the trajectories are optimized for both maneuver options. After this neutral part, the trajectories diverge.

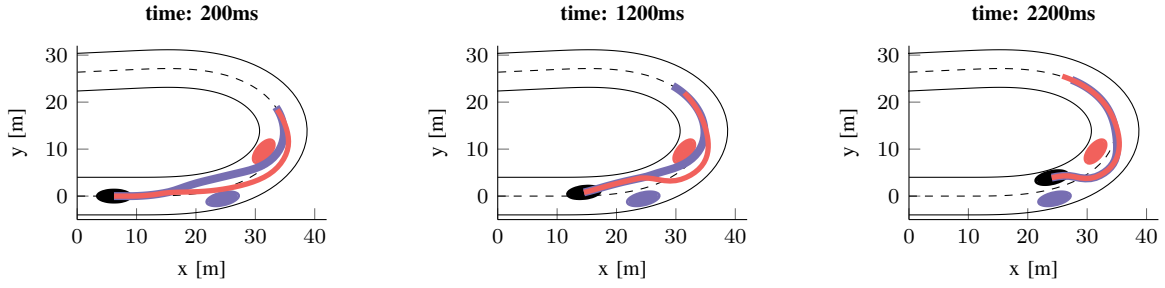


Figure 12: Simulation results for collision avoidance with two obstacles during a 180°-cornering. The motion profiles exhibit similar features to those in the previous figure.

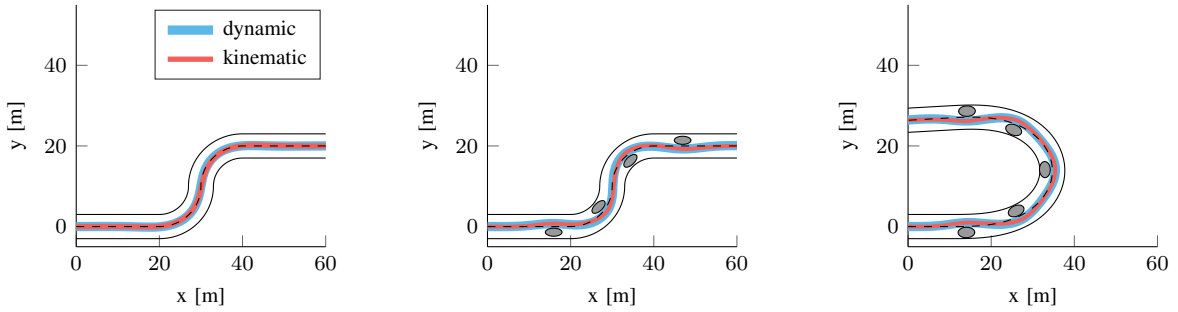


Figure 13: Scenarios for vehicle model simulations. Motion profiles for a dynamic bicycle model incorporating a linear tire model are compared with those from kinematic vehicle model. The first scenario is an S-shaped curve free of obstacles, the second scenario is the same but with obstacles, and the third scenario is 180°-cornering with obstacles.

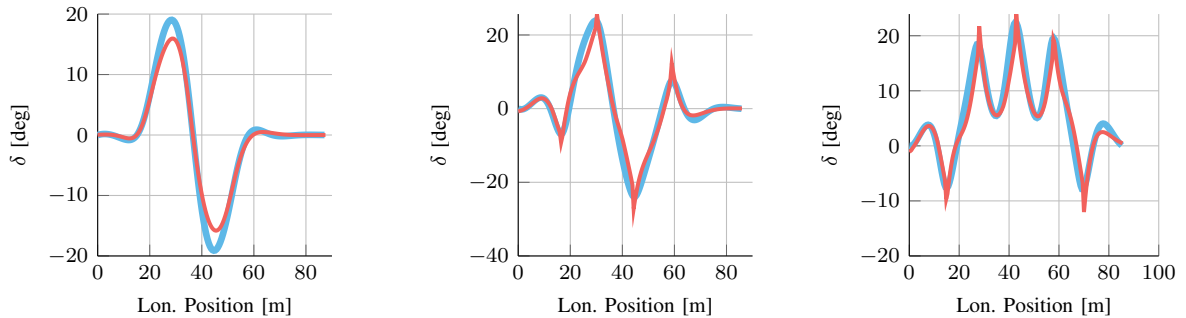


Figure 14: Comparison of steering angles  $\delta$  for the scenarios tested in the previous figure, presented in the same order. The color scheme for the vehicle models remains the same.

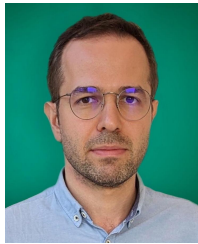
## REFERENCES

- [1] Ö. Ş. Taş, “Motion Planning for Autonomous Vehicles in Partially Observable Environments,” Ph.D. dissertation, Karlsruhe Institute of Technology, 2022.
- [2] D. González, J. Pérez, V. Milanés, and F. Nashashibi, “A Review of Motion Planning Techniques for Automated Vehicles,” *IEEE Transactions on Intelligent Transportation Systems*, vol. 17, no. 4, pp. 1135–1145, 2015.
- [3] B. Paden, M. Čáp, S. Z. Yong, D. Yershov, and E. Frazzoli, “A Survey of Motion Planning and Control Techniques for Self-driving Urban Vehicles,” *IEEE Transactions on Intelligent Vehicles*, vol. 1, no. 1, pp. 33–55, 2016.
- [4] F. Sana, N. L. Azad, and K. Raahemifar, “Autonomous Vehicle Decision-Making and Control in Complex and Unconventional Scenarios — A Review,” *Machines*, vol. 11, no. 7, p. 676, 2023.
- [5] Ö. Ş. Taş and C. Stiller, “Tackling Existence Probabilities of Objects with Motion Planning for Automated Urban Driving,” 2020, arXiv: 2002.01254.
- [6] M. M. Minderhoud and P. H. Bovy, “Extended time-to-collision measures for road traffic safety assessment,” *Accident Analysis & Prevention*, vol. 33, no. 1, pp. 89–97, 2001.
- [7] J. Hillenbrand, A. Spieker, and K. Kroschel, “Efficient decision making for a multi-level collision mitigation system,” in *IEEE Intelligent Vehicles Symposium (IV)*, 2006, pp. 460–465.
- [8] Y. Zhang, E. K. Antonsson, and K. Grote, “A New Threat Assessment Measure for Collision Avoidance Systems,” in *IEEE International Conference on Intelligent Transportation Systems (ITSC)*, 2006, pp. 968–975.
- [9] J. Hillenbrand, “Fahrerassistenz zur Kollisionsvermeidung,” Ph.D. dissertation, Karlsruhe Institute of Technology, 2007.
- [10] J. Ward, G. Agamennoni, S. Worrall, and E. Nebot, “Vehicle Collision Probability Calculation for General Traffic Scenarios Under Uncertainty,” in *IEEE Intelligent Vehicles Symposium (IV)*, 2014, pp. 986–992.
- [11] A. Eidehall and L. Petersson, “Statistical Threat Assessment for General Road Scenes Using Monte Carlo Sampling,” *IEEE Transactions on Intelligent Transportation Systems*, vol. 9, no. 1, pp. 137–147, 2008.
- [12] A. Berthelot, A. Tamke, T. Dang, and G. Breuel, “Handling uncertainties in criticality assessment,” in *IEEE Intelligent Vehicles Symposium (IV)*, 2011, pp. 571–576.
- [13] —, “A novel approach for the probabilistic computation of Time-To-Collision,” in *IEEE Intelligent Vehicles Symposium (IV)*, 2012, pp. 1173–1178.
- [14] J. E. Stellet, J. Schumacher, W. Branz, and J. M. Zöllner, “Uncertainty propagation in criticality measures for driver assistance,” in *IEEE Intelligent Vehicles Symposium (IV)*, 2015, pp. 1187–1194.
- [15] J. E. Stellet, P. Vogt, J. Schumacher, W. Branz, and J. M. Zöllner, “Analytical derivation of performance bounds of autonomous emergency brake systems,” in *IEEE Intelligent Vehicles Symposium (IV)*, 2016, pp. 220–226.
- [16] J. F. Medina-Lee, J. Godoy, A. Artuñedo, and J. Villagra, “Speed Profile Generation Strategy for Efficient Merging of Automated Vehicles on Roundabouts With Realistic Traffic,” *IEEE Transactions on Intelligent Vehicles*, vol. 8, no. 3, pp. 2448–2462, 2023.
- [17] J. Schulman, Y. Duan, J. Ho, A. Lee, I. Awwal, H. Bradlow, J. Pan, S. Patil, K. Goldberg, and P. Abbeel, “Motion Planning with Sequential Convex Optimization and Convex Collision Checking,” *International Journal of Robotics Research*, vol. 33, no. 9, pp. 1251–1270, 2014.
- [18] J. Ziegler and C. Stiller, “Fast Collision Checking for Intelligent Vehicle Motion Planning,” in *IEEE Intelligent Vehicles Symposium (IV)*, 2010, pp. 518–522.
- [19] J. Ziegler, P. Bender, T. Dang, and C. Stiller, “Trajectory Planning for Bertha — a Local, Continuous Method,” in *IEEE Intelligent Vehicles Symposium (IV)*, 2014, pp. 450–457.
- [20] M. Althoff, O. Stursberg, and M. Buss, “Online Verification of Cognitive Car Decisions,” in *IEEE Intelligent Vehicles Symposium (IV)*, 2007, pp. 728–733.
- [21] —, “Safety Assessment of Autonomous Cars using Verification Techniques,” in *American Control Conference (ACC)*, 2007, pp. 4154–4159.
- [22] B. Brito, B. Floor, L. Ferranti, and J. Alonso-Mora, “Model Predictive Contouring Control for Collision Avoidance in Unstructured Dynamic Environments,” *IEEE Robotics and Automation Letters*, vol. 4, no. 4, pp. 4459–4466, 2019.
- [23] G. C. Calafiore and L. El Ghaoui, “On Distributionally Robust Chance-Constrained Linear Programs,” *Journal of Optimization Theory and Applications*, vol. 130, no. 1, pp. 1–22, 2006.
- [24] L. Blackmore, H. Li, and B. Williams, “A Probabilistic Approach to Optimal Robust Path Planning with Obstacles,” in *American Control Conference (ACC)*, 2006, pp. 2831–2837.
- [25] A. Charnes and W. W. Cooper, “Deterministic Equivalents for Optimizing and Satisficing under Chance Constraints,” *Operations Research*, vol. 11, no. 1, pp. 18–39, 1963.
- [26] A. Majumdar and M. Pavone, “How Should a Robot Assess Risk? Towards an Axiomatic Theory of Risk in Robotics,” in *International Symposium of Robotic Research (ISRR)*, N. M. Amato, G. Hager, S. L. Thomas, and M. Torres-Torriti, Eds., 2017, pp. 75–84.
- [27] S. Shalev-Shwartz, S. Shammah, and A. Shashua, “On a Formal Model of Safe and Scalable Self-driving Cars,” 2017, arXiv: 1708.06374.
- [28] T. Nyberg, C. Pek, L. Dal Col, C. Norén, and J. Tumova, “Risk-aware motion planning for autonomous vehicles with safety specifications,” in *IEEE Intelligent Vehicles Symposium (IV)*, 2021, pp. 1016–1023.
- [29] M. Naumann, F. Wirth, F. Oboril, K.-U. Scholl, M. Soledad Elli, I. Alvarez, J. Weast, and C. Stiller, “On Responsibility Sensitive Safety in Car-following Situations - A Parameter Analysis on German Highways,” in *IEEE Intelligent Vehicles Symposium (IV)*, 2021, pp. 83–90.
- [30] B. Luders, M. Kothari, and J. How, “Chance Constrained RRT for Probabilistic Robustness to Environmental Uncertainty,” in *AIAA Guidance, Navigation, and Control Conference*, 2010, p. 8160.
- [31] G. S. Aoude, B. D. Luders, J. M. Joseph, N. Roy, and J. P. How, “Probabilistically Safe Motion Planning to Avoid Dynamic Obstacles with Uncertain Motion Patterns,” *Autonomous Robots*, vol. 35, no. 1, pp. 51–76, 2013.
- [32] A. Artuñedo, J. Villagra, J. Godoy, and M. D. Del Castillo, “Motion Planning Approach Considering Localization Uncertainty,” *IEEE Transactions on Vehicular Technology*, vol. 69, no. 6, pp. 5983–5994, 2020.
- [33] M. P. Vitus and C. J. Tomlin, “On Feedback Design and Risk Allocation in Chance Constrained Control,” in *IEEE Conference on Decision and Control (CDC)*, 2011, pp. 734–739.
- [34] —, “A Probabilistic Approach to Planning and Control in Autonomous Urban Driving,” in *IEEE Conference on Decision and Control (CDC)*, 2013, pp. 2459–2464.
- [35] A. Carvalho, Y. Gao, S. Lefevre, and F. Borrelli, “Stochastic Predictive Control of Autonomous Vehicles in Uncertain Environments,” in *International Symposium on Advanced Vehicle Control*, 2014, pp. 712–719.
- [36] D. Lenz, T. Kessler, and A. Knoll, “Stochastic Model Predictive Controller with Chance Constraints for Comfortable and Safe Driving Behavior of Autonomous Vehicles,” in *IEEE Intelligent Vehicles Symposium (IV)*, 2015, pp. 292–297.
- [37] G. R. de Campos, A. H. Runarsson, F. Granum, P. Falcone, and K. Alenljung, “Collision avoidance at intersections: A probabilistic threat-assessment and decision-making system for safety interventions,” in *IEEE International Conference on Intelligent Transportation Systems (ITSC)*, 2014, pp. 649–654.
- [38] V. Lefkopoulou and M. Kamgarpour, “Trajectory Planning Under Environmental Uncertainty with Finite-Sample Safety Guarantees,” *Automatica*, vol. 131, p. 109754, 2021.
- [39] P. F. Orzechowski, A. Meyer, and M. Lauer, “Tackling occlusions & limited sensor range with set-based safety verification,” in *IEEE International Conference on Intelligent Transportation Systems (ITSC)*, 2018, pp. 1729–1736.
- [40] E. Debada, A. Ung, and D. Gillet, “Occlusion-aware motion planning at roundabouts,” *IEEE Transactions on Intelligent Vehicles*, vol. 6, no. 2, pp. 276–287, 2020.
- [41] J. M. G. Sánchez, T. Nyberg, C. Pek, J. Tumova, and M. Törngren, “Foresee the unseen: Sequential reasoning about hidden obstacles for safe driving,” in *IEEE Intelligent Vehicles Symposium (IV)*, 2022, pp. 255–264.
- [42] S. Petti and T. Fraichard, “Safe Motion Planning in Dynamic Environments,” in *IEEE/RSJ International Conference on Intelligent Robots and Systems (IROS)*, 2005, pp. 2210–2215.
- [43] S. Magdici and M. Althoff, “Fail-Safe Motion Planning of Autonomous Vehicles,” in *IEEE International Conference on Intelligent Transportation Systems (ITSC)*, 2016, pp. 452–458.
- [44] Ö. Ş. Taş and C. Stiller, “Limited Visibility and Uncertainty Aware Motion Planning for Automated Driving,” in *IEEE Intelligent Vehicles Symposium (IV)*, 2018, pp. 1171–1178.
- [45] C. Pek and M. Althoff, “Computationally Efficient Fail-safe Trajectory Planning for Self-driving Vehicles Using Convex Optimization,” in *IEEE International Conference on Intelligent Transportation Systems (ITSC)*, 2018, pp. 1447–1454.
- [46] T. Brüdigam, M. Olbrich, D. Wollherr, and M. Leibold, “Stochastic Model Predictive Control with a Safety Guarantee for Automated

- Driving,” *IEEE Transactions on Intelligent Vehicles*, vol. 8, no. 1, pp. 22–36, 2023.
- [47] J. P. Alsterda, M. Brown, and J. C. Gerdes, “Contingency model predictive control for automated vehicles,” in *American Control Conference (ACC)*, 2019, pp. 717–722.
- [48] R. Oliveira, S. H. Nair, and B. Wahlberg, “Interaction and decision making-aware motion planning using branch model predictive control,” in *IEEE Intelligent Vehicles Symposium (IV)*, 2023.
- [49] M.-Y. Yu, R. Vasudevan, and M. Johnson-Roberson, “Occlusion-Aware Risk Assessment for Autonomous Driving in Urban Environments,” *IEEE Robotics and Automation Letters*, vol. 4, no. 2, pp. 2235–2241, 2019.
- [50] L. Wang, C. Burger, and C. Stiller, “Reasoning about Potential Hidden Traffic Participants by Tracking Occluded Areas,” in *IEEE International Conference on Intelligent Transportation Systems (ITSC)*, 2021, pp. 157–163.
- [51] H. Andersen, J. Alonso-Mora, Y. H. Eng, D. Rus, and M. H. Ang, “Trajectory Optimization and Situational Analysis Framework for Autonomous Overtaking With Visibility Maximization,” *IEEE Transactions on Intelligent Vehicles*, vol. 5, no. 1, pp. 7–20, 2019.
- [52] D. Sadigh, S. S. Sastry, S. A. Seshia, and A. Dragan, “Information Gathering Actions over Human Internal State,” in *IEEE/RSJ International Conference on Intelligent Robots and Systems (IROS)*, 2016, pp. 66–73.
- [53] S. Ulbrich and M. Maurer, “Probabilistic Online POMDP Decision Making for Lane Changes in Fully Automated Driving,” in *IEEE International Conference on Intelligent Transportation Systems (ITSC)*, 2013, pp. 2063–2067.
- [54] S. Brechtel, T. Gindele, and R. Dillmann, “Probabilistic Decision-Making under Uncertainty for Autonomous Driving using Continuous POMDPs,” in *IEEE International Conference on Intelligent Transportation Systems (ITSC)*, 2014, pp. 392–399.
- [55] C. Hubmann, J. Schulz, M. Becker, D. Althoff, and C. Stiller, “Automated Driving in Uncertain Environments: Planning With Interaction and Uncertain Maneuver Prediction,” *IEEE Transactions on Intelligent Vehicles*, vol. 3, no. 1, pp. 5–17, 2018.
- [56] M. Bouton, A. Nakhaei, K. Fujimura, and M. J. Kochenderfer, “Scalable Decision Making with Sensor Occlusions for Autonomous Driving,” in *IEEE International Conference on Robotics and Automation (ICRA)*, 2018, pp. 2076–2081.
- [57] C. Hubmann, N. Quetschlich, J. Schulz, J. Bernhard, D. Althoff, and C. Stiller, “A POMDP Maneuver Planner For Occlusions in Urban Scenarios,” in *IEEE Intelligent Vehicles Symposium (IV)*, 2019, pp. 2172–2179.
- [58] K. H. Wray, B. Lange, A. Jamgochian, S. J. Witwicki, A. Kobashi, S. Hagaribommanahalli, and D. Ilstrup, “POMDPs for Safe Visibility Reasoning in Autonomous Vehicles,” in *IEEE International Conference on Intelligence and Safety for Robotics (ISR)*, 2021, pp. 191–195.
- [59] Ö. Ş. Taş, F. Hauser, and M. Lauer, “Efficient Sampling in POMDPs with Lipschitz Bandits for Motion Planning in Continuous Spaces,” in *IEEE Intelligent Vehicles Symposium (IV)*, 2021, pp. 1081–1088.
- [60] W. Zeng, W. Luo, S. Suo, A. Sadat, B. Yang, S. Casas, and R. Urtasun, “End-to-end Interpretable Neural Motion Planner,” in *IEEE Computer Society Conference on Computer Vision and Pattern Recognition (CVPR)*, 2019, pp. 8660–8669.
- [61] S. Casas, A. Sadat, and R. Urtasun, “MP3: A Unified Model to Map, Perceive, Predict and Plan,” in *IEEE Computer Society Conference on Computer Vision and Pattern Recognition (CVPR)*, 2021, pp. 14403–14412.
- [62] D. Kamran, T. Engelgeh, M. Busch, J. Fischer, and C. Stiller, “Minimizing Safety Interference for Safe and Comfortable Automated Driving with Distributional Reinforcement Learning,” in *IEEE/RSJ International Conference on Intelligent Robots and Systems (IROS)*, 2021, pp. 1236–1243.
- [63] P. Bender, J. Ziegler, and C. Stiller, “Lanelets: Efficient Map Representation for Autonomous Driving,” in *IEEE Intelligent Vehicles Symposium (IV)*, 2014, pp. 420–425.
- [64] F. Poggenhans and J. Janosovits, “Pathfinding and Routing for Automated Driving in the Lanelet2 Map Framework,” in *IEEE International Conference on Intelligent Transportation Systems (ITSC)*, 2020, pp. 1–7.
- [65] Ö. Ş. Taş, “Integrating Combinatorial Reasoning and Continuous Methods for Optimal Motion Planning of Autonomous Vehicles,” Master’s thesis, Karlsruhe Institute of Technology, 2014.
- [66] S. Lefèvre, D. Vasquez, and C. Laugier, “A survey on motion prediction and risk assessment for intelligent vehicles,” *Robomech Journal*, vol. 1, no. 1, p. 1, 2014.
- [67] K. Brown, K. R. Driggs-Campbell, and M. J. Kochenderfer, “A Taxonomy and Review of Algorithms for Modeling and Predicting Human Driver Behavior,” 2020, arXiv: 2006.08832.
- [68] P. Bender, Ö. Ş. Taş, J. Ziegler, and C. Stiller, “The Combinatorial Aspect of Motion Planning: Maneuver Variants in Structured Environments,” in *IEEE Intelligent Vehicles Symposium (IV)*, 2015, pp. 1386–1392.
- [69] J. Park, S. Karumanchi, and K. Iagnemma, “Homotopy-based divide-and-conquer strategy for optimal trajectory planning via mixed-integer programming,” *IEEE Transactions on Robotics*, vol. 31, no. 5, pp. 1101–1115, 2015.
- [70] V. Z. Patterson, F. E. Lewis, and J. C. Gerdes, “Optimal decision making for automated vehicles using homotopy generation and nonlinear model predictive control,” in *IEEE Intelligent Vehicles Symposium (IV)*, 2021, pp. 1045–1050.
- [71] F. Althé and A. De La Fortelle, “Partitioning of the Free Space-Time for On-Road Navigation of Autonomous Ground Vehicles,” in *IEEE Conference on Decision and Control (CDC)*, 2017, pp. 2126–2133.
- [72] X. Qian, F. Althé, P. Bender, C. Stiller, and A. de La Fortelle, “Optimal trajectory planning for autonomous driving integrating logical constraints: An MIQP perspective,” in *IEEE International Conference on Intelligent Transportation Systems (ITSC)*, 2016, pp. 205–210.
- [73] C. Burger and M. Lauer, “Cooperative Multiple Vehicle Trajectory Planning using MIQP,” in *IEEE International Conference on Intelligent Transportation Systems (ITSC)*, 2018, pp. 602–607.
- [74] W. F. Milliken, D. L. Milliken, and L. D. Metz, *Race Car Vehicle Dynamics*. Warrendale, PA: SAE International, 1995.
- [75] P. Polack, F. Althé, B. d’Andréa Novel, and A. de La Fortelle, “The kinematic bicycle model: A consistent model for planning feasible trajectories for autonomous vehicles,” in *IEEE Intelligent Vehicles Symposium (IV)*, 2017, pp. 812–818.
- [76] J. Y. Goh, T. Goel, and C. J. Gerdes, “Toward Automated Vehicle Control Beyond the Stability Limits: Drifting Along a General Path,” *Journal of Dynamic Systems, Measurement and Control*, vol. 142, no. 2, p. 021004, 2020.
- [77] Ö. Ş. Taş, N. O. Salscheider\*, F. Poggenhans\*, S. Wirges\*, C. Bändera\*, M. R. Zofka\*, T. Strauss\*, J. M. Zöllner\*, and C. Stiller\*, “Making Bertha Cooperate - Team AnnieWAY’s Entry to the 2016 Grand Cooperative Driving Challenge,” *IEEE Transactions on Intelligent Transportation Systems*, vol. 19, no. 4, pp. 1262–1276, 2018.
- [78] J. T. Barron, “A General and Adaptive Robust Loss Function,” in *IEEE Computer Society Conference on Computer Vision and Pattern Recognition (CVPR)*, 2019, pp. 4331–4339.
- [79] W. Schwarting, J. Alonso-Mora, L. Paull, S. Karaman, and D. Rus, “Safe Nonlinear Trajectory Generation for Parallel Autonomy With a Dynamic Vehicle Model,” *IEEE Transactions on Intelligent Transportation Systems*, vol. 19, no. 9, pp. 2994–3008, 2017.
- [80] A. Liniger, A. Domahidi, and M. Morari, “Optimization-Based Autonomous Racing of 1:43 Scale RC Cars,” *Optimal Control Applications and Methods*, vol. 36, no. 5, pp. 628–647, 2015.
- [81] Ö. Ş. Taş, F. Hauser, and C. Stiller, “Decision-time Postponing Motion Planning for Combinatorial Uncertain Maneuvering,” in *IEEE International Conference on Intelligent Transportation Systems (ITSC)*, 2018, pp. 2419–2425.
- [82] B. T. Lopez, J.-J. E. Slotine, and J. P. How, “Dynamic tube mpc for nonlinear systems,” in *American Control Conference (ACC)*, 2019, pp. 1655–1662.
- [83] M. J. Kochenderfer and T. A. Wheeler, *Algorithms for Optimization*. Cambridge, MA, USA: MIT Press, 2019.
- [84] M. Wright, “The interior-point revolution in optimization: history, recent developments, and lasting consequences,” *Bulletin of the American Mathematical Society*, vol. 42, no. 1, pp. 39–56, 2005.
- [85] J. Nocedal and S. Wright, *Numerical Optimization*. New York, NY, USA: Springer Science & Business Media, 2006.
- [86] A. Wächter and L. T. Biegler, “On the implementation of an interior-point filter line-search algorithm for large-scale nonlinear programming,” *Mathematical Programming*, vol. 106, no. 1, pp. 25–57, 2006.
- [87] A. G. Baydin, B. A. Pearlmutter, A. A. Radul, and J. M. Siskind, “Automatic Differentiation in Machine Learning: a Survey,” *Journal of Machine Learning Research*, vol. 18, no. 1, pp. 5595–5637, 2018.
- [88] B. Bell, “CppAD: a package for C++ algorithmic differentiation,” 2021, <https://coin-or.github.io/CppAD/doc/cppad.htm>.
- [89] J. A. E. Andersson, J. Gillis, G. Horn, J. B. Rawlings, and M. Diehl, “CasADi – A software framework for nonlinear optimization and optimal control,” *Mathematical Programming Computation*, vol. 11, no. 1, pp. 1–36, 2019.



- [90] M. Gifftthaler, M. Neunert, M. Stäuble, and J. Buchli, “The Control Toolbox — An Open-Source C++ Library for Robotics, Optimal and Model Predictive Control,” in *IEEE International Conference on Simulation, Modeling, and Programming for Autonomous Robots (SIMPAN)*, 2018, pp. 123–129.
- [91] M. Neunert, M. Gifftthaler, M. Frigerio, C. Semini, and J. Buchli, “Fast Derivatives of Rigid Body Dynamics for Control, Optimization and Estimation,” in *IEEE International Conference on Simulation, Modeling, and Programming for Autonomous Robots (SIMPAN)*, 2016, pp. 91–97.
- [92] João Rui Leal, “CppADCodeGen,” 2017, <https://github.com/joaoleal/CppADCodeGen>, DOI: 10.5281/zenodo.836832.
- [93] R. Kohlhaas, T. Schamm, D. Lenk, and J. M. Zöllner, “Towards driving autonomously: Autonomous cruise control in urban environments,” in *IEEE Intelligent Vehicles Symposium (IV)*, 2013, pp. 109–114.
- [94] Ö. Ş. Taş, “P3IV: Probabilistic Prediction and Planning for Intelligent Vehicles Simulator,” 2021, <https://github.com/fzi-forschungszentrum-informatik/P3IV>.
- [95] W. Zhan, L. Sun, D. Wang, H. Shi, A. Clausse, M. Naumann, J. Kümmerle, H. Königshof, C. Stiller, A. de La Fortelle, and M. Tomizuka, “INTERACTION Dataset: An INTERnational, Adversarial and Cooperative moTION Dataset in Interactive Driving Scenarios with Semantic Maps,” 2019, arXiv: 1910.03088.
- [96] P. Amestoy, A. Buttari, J.-Y. L’Excellent, and T. Mary, “Performance and Scalability of the Block Low-Rank Multifrontal Factorization on Multicore Architectures,” *ACM Transactions on Mathematical Software*, vol. 45, no. 1, pp. 1–26, 2019.
- [97] “HSL. A collection of Fortran codes for large scale scientific computation,” 2013, <http://www.hsl.rl.ac.uk>.



**Ömer Şahin Taş** received his B.Sc. degree and an extracurricular minor from Istanbul Technical University, followed by M.Sc. and Ph.D. degrees from the Karlsruhe Institute of Technology (KIT), with “very good” and “summa cum laude” distinctions respectively. Upon completing his Ph.D., he spent three months at the University of Toronto as a visiting researcher, specializing in deep reinforcement learning. During his undergraduate studies, he pioneered the first Formula SAE/Student team in Turkey. He also participated in the Grand Cooperative Driving Challenge 2011 as a member of Team Mekar. In the Grand Cooperative Driving Challenge 2016, together with his team AnnieWAY, he

placed second. Since 2017, he is the head of the Mobile Perception Systems department at FZI Forschungszentrum Informatik.



**Philipp Heinrich Brusius** received the M.Sc. degree in mechanical engineering from the Karlsruhe Institute of Technology in 2021. He is currently working for Porsche Motorsport of Dr. Ing. h.c. F. Porsche AG, as part of the Vehicle Science group. His work includes the development of simulation methods for the vehicle dynamics analysis.



**Christoph Stiller** studied electrical engineering toward Diploma degree in Aachen, Germany, and Trondheim, Norway. He received the Dr.-Ing. (Ph.D.) from RWTH Aachen University in 1994 and spent a postdoc year at INRS in Montreal, Canada. In 1995, he joined the Corporate Research and Advanced Development of Robert Bosch GmbH, Hildesheim, Germany. In 2001, he became Chaired Professor at KIT, Germany. He was invited several prestigious universities for extended periods. In 2010, he spent three months by invitation at CSIRO in Brisbane, Australia, followed by a four-month sabbatical in 2015 with Bosch RTC and Stanford University in California. In 2023, he spent on a six-month sabbatical at the University of California, Berkeley. He served as the President of the IEEE Intelligent Transportation Systems Society (2012–2013) and was Vice President before since 2006. He served as the Editor-in-Chief of the IEEE Intelligent Transportation Systems Magazine (2009–2011) and as Associate Editor for the IEEE Transactions on Image Processing (1999–2003), for the IEEE Transactions on Intelligent Transportation Systems (2004–ongoing), and for the IEEE Intelligent Transportation Systems Magazine (2012–ongoing). His Autonomous Vehicle AnnieWAY was a finalist in the Urban Challenge 2007 and the winner and second winner of the Grand Cooperative Driving Challenge 2011 and 2016, respectively. In 2013, he collaborated with Daimler on the automated Bertha Benz Memorial Tour.